Precision of Flow Sensing by Self-Communicating Cells

Sean Fancher,[1,2] Michael Vennettilli,[1] Nicholas Hilgert,[1] and Andrew Mugler[1,*]

[1]*Department of Physics and Astronomy, Purdue University, West Lafayette, Indiana 47907, USA*
[2]*Department of Physics and Astronomy, University of Pennsylvania, Philadelphia, Pennsylvania 19104, USA*

Metastatic cancer cells detect the direction of lymphatic flow by self-communication: they secrete and detect a chemical which, due to the flow, returns to the cell surface anisotropically. The secretion rate is low, meaning detection noise may play an important role, but the sensory precision of this mechanism has not been explored. Here we derive the precision of flow sensing for two ubiquitous detection methods: absorption vs reversible binding to surface receptors. We find that binding is more precise due to the fact that absorption distorts the signal that the cell aims to detect. Comparing to experiments, our results suggest that the cancer cells operate remarkably close to the physical detection limit. Our prediction that cells should bind the chemical reversibly, not absorb it, is supported by endocytosis data for this ligand-receptor pair.

Metastasis is the process of cancer cells spreading from the primary tumor to other parts of the body. A major route for spreading is the lymphatic system, a network of vessels that carry fluid to the heart. Particular cancer cells detect the drainage of lymphatic fluid toward the vessels and move in that direction [1]. Experiments have shown that the detection occurs by self-communication: the cells secrete diffusible molecules (CCL19 and CCL21) that they detect with receptors (CCR7) on their surface [2]. The flow affects the distribution of detected molecules, which thereby provides information about the flow direction. This flow detection mechanism, termed "autologous chemotaxis," has been observed for breast cancer [2], melanoma [2], and glioma cell lines [3], as well as endothelial cells [4], and has been studied using fluid dynamics models [2,5,6].

The flow is slow. Lymphatic drainage speeds near tumors are typically $v_0 = 0.1$–$1 \ \mu$m/s [7,8], and the speed decreases further with proximity to the cell surface due to the laminar nature of low-Reynolds-number flow. In contrast, a secreted molecule diffuses with coefficient $D = 130$–$160 \ \mu$m^2/s [5], covering a distance equivalent to the cell radius ($a \approx 10 \ \mu$m [2]) in a typical time of a^2/D and giving a "velocity" of $D/a = 13$–$16 \ \mu$m/s. The ratio of these velocities $\epsilon \equiv v_0 a/D = 0.006$–$0.08$, called the Péclet number, is small, indicating that diffusion dominates over flow in this process.

Also, the secretion rate is low. Cells secrete 0.7–2.3×10^{-15} g of CCL19 and CCL21 in a 24-hour period (Fig. 3F in Ref. [2]), which given the molecular weights of these ligands (11 and 14.6 kDa, respectively [9]), corresponds to a secretion rate of $\nu = 1200$–5200 molecules per hour. Yet, cells begin migrating in a matter of hours [2].

The slow flow and low secretion rate raise the question of whether autologous chemotaxis is a physically plausible mechanism for these cells. Is a couple thousand molecules, biased by such a weak flow field, enough to determine the flow direction? If so, with what precision? Although this mechanism has been modeled at the continuum level, the question of sensory precision has remained unexplored.

At the same time, the question of sensory precision has been heavily explored for other cellular processes, beginning with the early work of Berg and Purcell [10], and extending to more modern works on concentration sensing [11–18], gradient sensing [19–23], and related sensory tasks [24–27]. Yet, the mechanism of autologous chemotaxis has thus far evaded this list, despite its importance to cancer biology and its potential for interesting physics.

Here we combine stochastic techniques from sensory biophysics with perturbation techniques from fluid dynamics to derive the fundamental limit to the precision of flow sensing by self-communication. We consider two ubiquitous methods of molecule detection: absorption vs reversible binding to receptors (Fig. 1). For both, we find a Berg-Purcell–like expression that is ultimately limited by the Péclet number, the secretion rate, and the integration time. Comparing to the experiments, this expression places a stringent limit on the level of precision that is possible for these cells, suggesting that they detect the flow direction near optimally given the physical constraints. Finally, we predict that reversible binding is more precise than absorption due to the fact that absorption necessarily reduces the anisotropy in the detected signal, a prediction that we test with endocytosis data.

Consider a spherical cell with radius a that secretes molecules isotropically with rate $\beta \equiv \nu/4\pi a^2$ per unit area, in the presence of a fluid flowing with velocity v_0 (Fig. 1). At low Reynolds number and high environmental permeability, laminar flow lines obeying Stokes' equation [10]
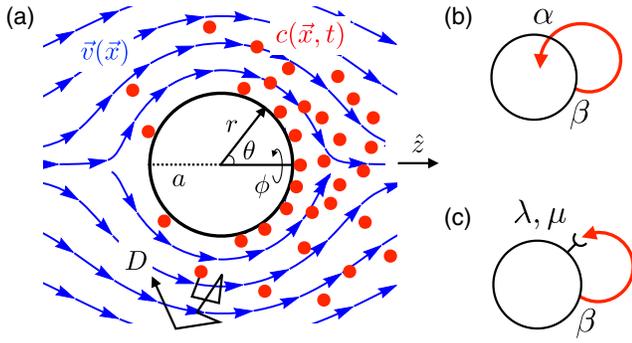
FIG. 1. Flow sensing by self-communication. (a) A cell isotropically secretes molecules (red) that diffuse and drift along laminar flow lines (blue). The cell detects the molecules by (b) absorption or (c) reversible binding to receptors.

form around the cell [Fig. 1(a), blue]. However, in the tumor environment and in experiments, the permeability $\mathcal{K}$ is low ($\kappa \equiv \sqrt{\mathcal{K}}/a \sim 10^{-3}$ [2]), and the flow lines obey the more general Brinkman's equation [28]. For a sphere at steady state they are given by [29]

$$\vec{v}(r,\theta,\phi) = v_0 \cos\theta \left[1 - \frac{\zeta}{\rho^3} + \frac{3\kappa}{\rho^2}\left(1+\frac{\kappa}{\rho}\right)e^{-(\rho-1)/\kappa}\right]\hat{r}$$
$$- v_0 \sin\theta\left[1 + \frac{\zeta}{2\rho^3} - \frac{3}{2\rho}\left(1+\frac{\kappa}{\rho}+\frac{\kappa^2}{\rho^2}\right)e^{-(\rho-1)/\kappa}\right]\hat{\theta}.$$
(1)

Here, $\rho \equiv r/a$ and $\zeta \equiv 1 + 3\kappa + 3\kappa^2$, the flow is in the $\hat{z}$ direction ($\theta = 0$), $\hat{r}$ and $\hat{\theta}$ are the radial and polar unit vectors, and $\vec{v}$ is independent of ϕ by symmetry. In the limit $\kappa \to \infty$, Eq. (1) reduces to Stokes flow; we are interested in the opposite limit. Note that $\vec{v} = 0$ at the cell surface $r = a$.

The molecules diffuse with coefficient D and drift along the flow lines [Fig. 1(a), red]. This process creates a stochastically evolving concentration field $c(r,\theta,\phi,t)$ with a mean $\bar{c}(r,\theta,\phi,t)$, where the bar represents the ensemble average over many independent realizations of the system. The mean follows the diffusion-drift equation, which at steady state reads

$$0 = \frac{\partial\bar{c}}{\partial t} = D\nabla^2\bar{c} - \vec{v}\cdot\vec{\nabla}\bar{c}.$$
(2)

We consider two cases for molecule detection at the cell surface: absorption [Fig. 1(b)] or reversible receptor binding [Fig. 1(c)]. In the former, there exists a flux boundary condition at the cell surface,

$$-D\frac{\partial\bar{c}(r,\theta)}{\partial r}\bigg|_a = \beta - \alpha\bar{c}(a,\theta),$$
(3)

where α is the absorption rate per unit area, and $\bar{c}(r,\theta)$ is independent of ϕ and t by symmetry and the system being

in steady state, respectively. We also require that the concentration vanish at infinity.

We define the dimensionless concentration $\chi \equiv \bar{c}a^3$ and velocity $\vec{u} \equiv \vec{v}/v_0$. In terms of the dimensionless radial distance ρ and the Péclet number ϵ, Eq. (2) at steady state becomes $0 = \nabla^2_\rho\chi - \epsilon\vec{u}\cdot\vec{\nabla}_\rho\chi$. Because ϵ is small, we use a perturbative solution $\chi = \chi_0 + \epsilon\chi_1$. However, in problems with diffusion and background flow, a single perturbative expansion cannot simultaneously satisfy the boundary conditions at $r = a$ [Eq. (3)] and $r \to \infty$ ($\bar{c} \to 0$) due to the particular spatial nonuniformity of $\vec{u}$ [30]. The resolution is to split the solution into an inner part $\chi(\rho,\theta)$ that satisfies the boundary condition at the cell surface and holds when ρ is order one, and an outer part $X(s,\theta)$ that satisfies the boundary condition at infinity and holds when $s = \epsilon\rho$ is order one. We match χ and X by requiring them to be equal at each order in ϵ as $\rho \to \infty$ and $s \to 0$, respectively.

To zeroth order, the inner solution satisfies Laplace's equation, $0 = \nabla^2_\rho\chi_0$, the general solution to which consists of spherical harmonics and powers of ρ [31]. For the outer solution, we write Eq. (2) in terms of s and X, which reads $0 = \nabla^2_s X - \vec{u}\cdot\vec{\nabla}_s X$. One can define a perturbative expansion for X, but we show [31] that only the leading terms of X and $\vec{u}$ matter. The latter is $\vec{u} = \hat{z}$, corresponding to the uniform flow far from the cell where X applies. The solution to this equation satisfying $X \to 0$ as $s \to \infty$ consists of modified Bessel functions and spherical harmonics [31].

We find that the matching condition requires all but one term in χ_0 and X to vanish [31], yielding

$$\chi_0 = \frac{\gamma}{\rho}, \qquad X = \frac{\epsilon\gamma}{s}e^{-s(1-\cos\theta)/2},$$
(4)

where $\gamma \equiv \tilde{\beta}/(1+\tilde{\alpha})$, and $\tilde{\beta} \equiv \beta a^4/D$ and $\tilde{\alpha} \equiv \alpha a/D$ are dimensionless secretion and absorption rates, respectively. We see that to leading order, the concentration falls off with distance, and far from the cell it is largest in the flow direction ($\theta = 0$).

To obtain the anisotropy near the cell, which is essential for the flow sensing problem, we must go to the next order. χ_1 satisfies $0 = \nabla^2_\rho\chi_1 - \vec{u}\cdot\vec{\nabla}_\rho\chi_0$, which is the Poisson equation with $\vec{u}$ [Eq. (1)] and χ_0 [Eq. (4)] providing the source term. This equation can be solved using a Green's function, with coefficients determined by Eq. (3) and matching to X in Eq. (4) [31]. The result is

$$\chi_1 = \frac{\gamma}{2}\left\{\frac{\tilde{\alpha}}{(1+\tilde{\alpha})\rho} - 1 + \frac{\cos\theta}{4}\left[\frac{(1-\tilde{\alpha})w}{(2+\tilde{\alpha})\rho^2} + f(\rho,\kappa)\right]\right\},$$
(5)

where $w \equiv 1 + \kappa^{-1} - \kappa^{-2}e^{1/\kappa}E_1(\kappa^{-1})$ is a monotonic function that limits to 2 ($\kappa \ll 1$) and 1 ($\kappa \gg 1$), $f(\rho,\kappa)$ is an α-independent function [31], and $E_1(x) \equiv \int_1^\infty dt\, e^{-tx}/t$. We

see that χ_1 acquires a $\cos\theta$ anisotropy largest in the flow direction ($\theta = 0$). We have checked by numerical solution of Eq. (2) that for $\epsilon \leq 0.1$, Eq. (5) is accurate to within 0.4% at the cell surface [31,32].

Information about the anisotropy, and thus the flow direction, comes from the front-back asymmetry in the absorptive flux of molecules αc at the cell surface over a time T, which is captured by weighing each absorption event by its location represented as $\cos\theta$. Normalizing this by the mean number of absorbed molecules, we define the anisotropy measure [19,23]

$$A \equiv \frac{\int_0^T dt \int a^2 d\Omega \alpha c(a,\theta,\phi,t) \cos\theta}{T \int a^2 d\Omega' \alpha \bar{c}(a,\theta')}, \qquad (6)$$

where $d\Omega = d\phi d\theta \sin\theta$, and the cosine extracts the asymmetry between the front ($\theta = 0$) and back ($\theta = \pi$). Using the solution for χ in Eqs. (4) and (5) and the fact that $f(1,\kappa) = w$, the mean evaluates to [31]

$$\bar{A} = \frac{w\epsilon}{8(2 + \tilde{\alpha})} \qquad (7)$$

to leading order in ϵ.

Equation (7) gives the mean anisotropy but ignores the counting noise due to diffusive molecule arrival. The equivalent expression to Eq. (6) that accounts for discrete molecule arrival is [19] $A = \bar{N}^{-1} \sum_{i=1}^{N} \cos\theta_i$, where θ_i is the arrival angle of the ith molecule, and $N = \int_0^T dt \int a^2 d\Omega \alpha c(a,\theta,\phi,t)$ is the total number of molecules absorbed in time T. The mean of this expression is given by Eq. (7) [31]. The variance is calculated by recognizing that molecule arrivals are statistically independent and that N is Poissonian [19] (which we have checked even with flow using particle-based simulations [31,32]). The result is [31]

$$\sigma_A^2 = \frac{1}{\bar{N}} = \frac{1}{\nu T}\left(\frac{1 + \tilde{\alpha}}{\tilde{\alpha}}\right) \qquad (8)$$

to leading order in ϵ. This expression includes [as does Eq. (14) below] a factor of 3 that arises from each directionally independent component of the variance. We see that the variance in the anisotropy scales inversely with the mean number of absorbed molecules.

Combining Eqs. (7) and (8), we obtain a relative error of

$$\frac{\sigma_A^2}{\bar{A}^2} = \frac{64(1 + \tilde{\alpha})(2 + \tilde{\alpha})^2}{w^2 \epsilon^2 \nu T \tilde{\alpha}} \gtrsim \frac{282}{\epsilon^2 \nu T}. \qquad (9)$$

In the second step, we have set w to its maximal value of 2 for $\kappa \ll 1$ (as in the experiments [2]) and recognized that the expression has a minimum at $\tilde{\alpha}^* = (\sqrt{17} - 1)/4 \approx 0.78$. The minimum arises from the following tradeoff: strong absorption maximizes the number of detected molecules and therefore reduces noise (Eq. (8); but it also

causes molecules to be absorbed immediately after release, preventing them from interacting with the nonzero flow away from the cell surface and therefore reducing the mean [Eq. (7)]. Equation (9) sets the fundamental limit to the precision of flow sensing by molecule absorption, dependent only on the Péclet number ϵ and the total number of secreted molecules νT.

We now consider the case of reversible receptor binding [Fig. 1(c)]. Calling $b(\theta,\phi,t)$ the surface concentration of bound receptors, we have

$$\frac{\partial c}{\partial t} = D\nabla^2 c - \vec{v} \cdot \vec{\nabla} c + \eta_D + \left(-\frac{\partial b}{\partial t} + \beta + \eta_\beta\right)\delta(r - a),$$

$$\frac{\partial b}{\partial t} = \lambda c(a,\theta,\phi,t) - \mu b + \eta_b, \qquad (10)$$

where the term proportional to the delta function contains the boundary condition at the surface. Here $\lambda \equiv k_a(R/4\pi a^2 - b) \approx k_a R/4\pi a^2$ and μ are the binding and unbinding rates, respectively, where k_a is the intrinsic ligand-receptor association rate, and R is the number of receptors per cell. Because binding is reversible, there are correlations between the bound receptor concentrations at different regions of the cell surface. Therefore, we cannot use the Poisson counting technique [Eq. (8)] to calculate the noise. Instead, we include Langevin noise terms in Eq. (10) to account for these correlations. These terms have zero mean, are uncorrelated with each other, and satisfy [18,23,33,34]

$$\langle \eta_D(\vec{r},t)\eta_D(\vec{r}',t')\rangle = 2D\delta(t - t')\vec{\nabla}_r \cdot \vec{\nabla}_{r'}[\bar{c}(\vec{r})\delta(\vec{r} - \vec{r}')],$$

$$\langle \eta_\beta(\Omega,t)\eta_\beta(\Omega',t')\rangle = \beta\delta(\Omega - \Omega')\delta(t - t'),$$

$$\langle \eta_b(\Omega,t)\eta_b(\Omega',t')\rangle = 2\mu\bar{b}\delta(\Omega - \Omega')\delta(t - t'), \qquad (11)$$

where $\bar{c}(r,\theta)$ and $\bar{b}(\theta) = \lambda\bar{c}(a,\theta)/\mu$ are the mean concentrations in steady state. Binding and unbinding equilibrate in steady state, such that $\bar{c}(r,\theta)$ is given by the previous solution [Eqs. (4) and (5)] but with $\alpha = 0$. The approximation in the definition of λ above neglects receptor saturation, which is valid because $\bar{c}(a)/K_d = \nu/4\pi aDK_d \sim 10^{-4}$, where we have used the isotropic approximation for $\bar{c}(a)$ [Eq. (4), $\alpha = 0$] and a dissociation constant of $K_d = \mu/k_a \sim 1$ nM for CCL19 and CCL21 binding to the CCR7 receptor [35,36].

In the reversible binding case, the anisotropy is defined as the average of the cosine over the angular distribution of bound receptors and the integration time T,

$$A \equiv \frac{\int_0^T dt \int a^2 d\Omega b(\theta,\phi,t) \cos\theta}{T \int a^2 d\Omega' \bar{b}(\theta')}. \qquad (12)$$

Because $\bar{b}(\theta) = \lambda\bar{c}(a,\theta)/\mu$, the means of Eqs. (6) and (12) take equivalent forms. Therefore, to leading order in ϵ, the mean of Eq. (12) is simply Eq. (7) with $\alpha = 0$,

$$\bar{A} = \frac{w\epsilon}{16}. \tag{13}$$

To solve Eqs. (10)–(12) for the variance, we Fourier transform them in space and time, calculate the power spectrum of A, and recognize that $\sigma_A^2 T$ is given by its low-frequency limit [11,18,22,23]. The result is [31]

$$\sigma_A^2 = \frac{1}{\nu T}\left(\frac{7}{9} + \frac{2}{\tilde{\lambda}}\right) \tag{14}$$

to leading order in ϵ, where $\tilde{\lambda} \equiv \lambda a/D$. The two terms are from noise due to (i) secretion and diffusion, and (ii) binding and unbinding, respectively. The derivation of Eq. (14) assumes that $T \gg \{\tau_1, \tau_2\}$, where $\tau_1 \equiv a^2/D \sim 1$ s is the characteristic time for a ligand molecule to diffuse across the cell, and $\tau_2 \equiv (1+\tilde{\lambda})/\mu \approx \tilde{\lambda}/\mu = R/4\pi a D K_d \sim$ 1–10 s is the receptor equilibration timescale [18]. For τ_2 we take $R \sim 10^4$–10^5 CCR7 receptors per cell [35,37] and $\tilde{\lambda} \gg 1$, which corresponds to diffusion-limited binding as further discussed below. Because cells migrate over hours, we see that $T \gg \{\tau_1, \tau_2\}$ should indeed be valid.

Combining Eqs. (13) and (14), we obtain the relative error

$$\frac{\sigma_A^2}{\bar{A}^2} = \frac{1792}{9w^2\epsilon^2\nu T}\left(1 + \frac{18}{7\tilde{\lambda}}\right) \gtrsim \frac{50}{\epsilon^2\nu T}. \tag{15}$$

In the second step, we again take $w = 2$ and $\tilde{\lambda} \gg 1$. Comparing Eqs. (9) and (15), we see that reversible binding achieves $\sqrt{282/50} \approx 2.4$ times lower error than absorption. The reason is that absorption [Eq. (7)], but not binding [Eq. (13)], reduces the anisotropy. Absorption is an active modifier of the signal created by secretion and flow, whereas reversible binding is a passive monitor.

How do our results compare to the experiments on metastatic cancer cells? The inequality in Eq. (15) provides the fundamental detection limit. We plot this expression as a function of T in Fig. 2 using the maximal experimental values of $\epsilon = 0.08$ and $\nu = 5200$/hr [2] to obtain the minimum possible error. We see that low errors are not possible in a few hours; even 10% error would take over 150 h to achieve. Yet, the cells are observed to migrate over a 15 h period [2]. In this time frame, it is not possible to achieve less than 30% error (Fig. 2). The situation is likely worse, given that the cells presumably begin migrating well before the 15-hour mark, and given that we have neglected any internal signaling noise. Thus, we see that the sensory performance is severely limited by the experimental parameters and the physics of the detection process. We conclude that these cells operate remarkably close to the fundamental detection limit.

We find that absorption is less precise than reversible binding [Eqs. (9) and (15)]. A ubiquitous mechanism of ligand absorption is endocytosis, wherein bound receptors
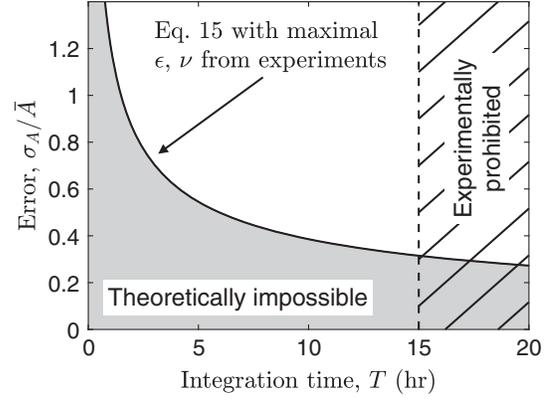
FIG. 2. Fundamental limit to the precision of flow sensing. Maximum experimental values $\epsilon = 0.08$ and $\nu = 5200$/hr [2] are used for minimum error (solid line). Cells migrate within 15 h [2] (dashed line). Lowest possible error is 30%.

are internalized into the cell. Therefore, we predict that the degree of CCR7 endocytosis in response to CCL19 and CCL21 binding is low. This prediction can be tested with endocytosis data on this ligand-receptor pair. Specifically, to achieve optimal absorption in Eq. (9) ($\tilde{\alpha}^* \approx 0.78$), absorption would need to occur at a rate of $4\pi a^2 \alpha^* \bar{c}(a) = \nu\tilde{\alpha}^*/(1+\tilde{\alpha}^*) \sim 25$ min^{-1}, where we have used the isotropic approximation for $\bar{c}(a)$ [Eq. (4)]. However, the rate of CCR7 endocytosis in response to CCL19 and CCL21 binding is many times slower at about 1 min^{-1} [38]. Thus, the degree of endocytosis is much lower than required for the absorption mechanism, as predicted.

We also find that reversible binding is most precise when the parameter $\tilde{\lambda} = Rk_a/4\pi aD$ is large [Eq. (15)]. Writing this parameter as $\tilde{\lambda} = (k_a/4\pi\ell D)(R\ell/a)$, where ℓ is the receptor length scale, we see that the first factor is the ratio that determines whether ligand-receptor binding is diffusion limited ($k_a \gg 4\pi\ell D$) or reaction limited ($k_a \ll 4\pi\ell D$). With the known values of R and a and a typical receptor length scale of $\ell \sim 10$ nm, the second factor evaluates to 10–100. Therefore, the requirement that $\tilde{\lambda} \gg 1$ is equivalent to the statement that binding is either diffusion limited or weakly reaction limited. Given the high sensory performance implied by Fig. 2 and the low degree of endocytosis found above, we thus predict that CCL19 and CCL21 binding to CCR7 is either diffusion limited or weakly reaction limited. We are not aware of kinetics data that would test this prediction.

Our finding that reversible binding is more precise than absorption is the opposite of what was found for the detection of an externally established concentration gradient [19]. The reason is that in our problem absorption removes molecules at the source, whereas in that problem molecules are replenished by a source at infinity. Depletion at the source prevents interactions with the flow and therefore weakens the anisotropy. Additionally, our models do not include any additional noise sources from processes

internal to the cell such as protein signaling or gene expression. Because any such process would simply add a fixed amount of noise, our finding is unaffected by the inclusion of internal dynamics, and Eq. (15) remains a theoretical minimum to the error in flow sensing.

The severity of the limit in Fig. 2 raises the question of whether metastatic cancer cells benefit from additional sensory mechanisms not accounted for in our modeling. The precision of flow sensing may be affected by geometric properties of the cell such as a nonuniform distribution of receptors or aspherical morphology. We find that receptor clustering has a negligible effect on the anisotropy but that an ellipsoidal cell [39,40] can decrease its sensory error by elongating in the direction of the flow [31,32]. Further investigation of the effects of cell geometry would be an interesting topic for future work. Some chemoattractants including CCL21 are known to bind to extracellular matrix fibers and be subsequently released by proteases [41–44]. This effect has been shown in continuum models of autologous chemotaxis to substantially increase the anisotropy [4,5], although the impact on the noise is unknown. It is also important to recognize that these cells do not perform flow sensing in isolation. Indeed, studies have shown that their migration is (i) increased in the presence of another cell type (fibroblasts) [45], (ii) decreased at high cell densities [46], and (iii) reversed at even higher cell densities (although reversal is attributed to a separate pressure-sensing mechanism) [46]. The extension of our work to multiple cells remains to be explored. Finally, recent work has highlighted the benefit of on-the-fly sensing [25,47], where an agent makes (and continually updates) its decision during the integration time, instead of afterward as assumed here. On-the-fly sensing may play an important role for these cells.

We have derived the fundamental limit to flow sensing by self-communication and shown that it strongly constrains the performance of metastatic cancer cells. Our work elucidates the physics behind a fascinating detection process and provides quantitative insights into a critical step in cancer progression.

---

*amugler@purdue.edu

[1] S. D. Nathanson, Insights into the mechanisms of lymph node metastasis, Cancer **98**, 413 (2003).

[2] J. D. Shields, M. E. Fleury, C. Yong, A. A. Tomei, G. J. Randolph, and M. A. Swartz, Autologous chemotaxis as a mechanism of tumor cell homing to lymphatics via interstitial flow and autocrine CCR7 signaling, Cancer Cell **11**, 526 (2007).

[3] J. M. Munson, R. V. Bellamkonda, and M. A. Swartz, Interstitial flow in a 3D microenvironment increases glioma invasion by a CXCR-4-dependent mechanism, Cancer Res. **73**, 1536 (2013).

[4] C.-L. E. Helm, M. E. Fleury, A. H. Zisch, F. Boschetti, and M. A. Swartz, Synergy between interstitial flow and VEGF directs capillary morphogenesis in vitro through a gradient amplification mechanism, Proc. Natl. Acad. Sci. U.S.A. **102**, 15779 (2005).

[5] M. E. Fleury, K. C. Boardman, and M. A. Swartz, Autologous morphogen gradients by subtle interstitial flow and matrix interactions, Biophys. J. **91**, 113 (2006).

[6] J. O. Waldeland and S. Evje, A multiphase model for exploring tumor cell migration driven by autologous chemotaxis, Chem. Eng. Sci. **191**, 268 (2018).

[7] S. R. Chary and R. K. Jain, Direct measurement of interstitial convection and diffusion of albumin in normal and neoplastic tissues by fluorescence photobleaching, Proc. Natl. Acad. Sci. U.S.A. **86**, 5385 (1989).

[8] H. Dafni, T. Israely, Z. M. Bhujwalla, L. E. Benjamin, and M. Neeman, Overexpression of vascular endothelial growth factor 165 drives peritumor interstitial convection and induces lymphatic drain: Magnetic resonance imaging, confocal microscopy, and histological tracking of triple-labeled albumin, Cancer Res. **62**, 6731 (2002).

[9] P. V. Hornbeck, B. Zhang, B. Murray, J. M. Kornhauser, V. Latham, and E. Skrzypek, PhosphoSitePlus, 2014: Mutations, PTMs and recalibrations, Nucleic Acids Res. **43**, D512 (2015).

[10] H. C. Berg and E. M. Purcell, Physics of chemoreception, Biophys. J. **20**, 193 (1977).

[11] W. Bialek and S. Setayeshgar, Physical limits to biochemical signaling, Proc. Natl. Acad. Sci. U.S.A. **102**, 10040 (2005).

[12] K. Wang, W.-J. Rappel, R. Kerr, and H. Levine, Quantifying noise levels of intercellular signals, Phys. Rev. E **75**, 061905 (2007).

[13] R. G. Endres and N. S. Wingreen, Maximum Likelihood and the Single Receptor, Phys. Rev. Lett. **103**, 158101 (2009).

[14] A. M. Berezhkovskii and A. Szabo, Effect of ligand diffusion on occupancy fluctuations of cell-surface receptors, J. Chem. Phys. **139**, 121910 (2013).

[15] K. Kaizu, W. De Ronde, J. Paijmans, K. Takahashi, F. Tostevin, and P. . Ten Wolde, The Berg-Purcell limit revisited, Biophys. J. **106**, 976 (2014).

[16] A. H. Lang, C. K. Fisher, T. Mora, and P. Mehta, Thermodynamics of Statistical Inference by Cells, Phys. Rev. Lett. **113**, 148103 (2014).

[17] B. A. Bicknell, P. Dayan, and G. J. Goodhill, The limits of chemosensation vary across dimensions, Nat. Commun. **6**, 7468 (2015).

[18] S. Fancher and A. Mugler, Fundamental Limits to Collective Concentration Sensing in Cell Populations, Phys. Rev. Lett. **118**, 078101 (2017).

[19] R. G. Endres and N. S. Wingreen, Accuracy of direct gradient sensing by single cells, Proc. Natl. Acad. Sci. U.S.A. **105**, 15749 (2008).

[20] R. G. Endres and N. S. Wingreen, Accuracy of direct gradient sensing by cell-surface receptors, Prog. Biophys. Molec. Biol. **100**, 33 (2009).

[21] B. Hu, W. Chen, W.-J. Rappel, and H. Levine, Physical Limits on Cellular Sensing of Spatial Gradients, Phys. Rev. Lett. **105**, 048104 (2010).

[22] A. Mugler, A. Levchenko, and I. Nemenman, Limits to the precision of gradient sensing with spatial communication and temporal integration, Proc. Natl. Acad. Sci. U.S.A. **113**, E689 (2016).

[23] J. Varennes, S. Fancher, B. Han, and A. Mugler, Emergent Versus Individual-Based Multicellular Chemotaxis, Phys. Rev. Lett. **119**, 188101 (2017).

[24] T. Mora and N. S. Wingreen, Limits of Sensing Temporal Concentration Changes by Single Cells, Phys. Rev. Lett. **104**, 248101 (2010).

[25] E. D. Siggia and M. Vergassola, Decisions on the fly in cellular sensory systems, Proc. Natl. Acad. Sci. U.S.A. **110**, E3704 (2013).

[26] T. Mora, Physical Limit to Concentration Sensing Amid Spurious Ligands, Phys. Rev. Lett. **115**, 038102 (2015).

[27] T. Mora and I. Nemenman, Physical Limit to Concentration Sensing in a Changing Environment, Phys. Rev. Lett. **123**, 198101 (2019).

[28] H. C. Brinkman, A calculation of the viscous force exerted by a flowing fluid on a dense swarm of particles, Flow Turbul. Combust. **1**, 27 (1949).

[29] B. Barman, Flow of a Newtonian fluid past an impervious sphere embedded in a porous medium, Indian J. Pure Appl. Math. **27**, 1249 (1996).

[30] A. Acrivos and T. D. Taylor, Heat and mass transfer from single spheres in Stokes flow, Phys. Fluids **5**, 387 (1962).

[31] See Supplemental Material at http://link.aps.org/supplemental/10.1103/PhysRevLett.124.168101 for additional derivations, numerical and simulation results, and extensions to nonuniform receptors and ellipsoidal cells.

[32] Code is available at https://github.com/nhilgert/flow-sensing.

[33] C. W. Gardiner, *Handbook of Stochastic Methods for Physics*, Chemistry and the Natural Sciences, 3rd ed. (Springer-Verlag, Berlin, 2004).

[34] D. T. Gillespie, The chemical Langevin equation, J. Chem. Phys. **113**, 297 (2000).

[35] K. Willimann, D. F. Legler, M. Loetscher, R. S. Roos, M. B. Delgado, I. Clark-Lewis, M. Baggiolini, and B. Moser, The chemokine SLC is expressed in T cell areas of lymph nodes and mucosal lymphoid tissues and attracts activated T cells via CCR7, European Journal of Immunology **28**, 2025 (1998).

[36] R. Yoshida, M. Nagira, M. Kitaura, N. Imagawa, T. Imai, and O. Yoshie, Secondary lymphoid-tissue chemokine is a functional ligand for the CC chemokine receptor CCR7, J. Biol. Chem. **273**, 7118 (1998).

[37] I. Comerford, S. Milasta, V. Morrow, G. Milligan, and R. Nibbs, The chemokine receptor CCX-CKR mediates effective scavenging of CCL19 *in vitro*, European Journal of Immunology **36**, 1904 (2006).

[38] M. A. Byers, P. A. Calloway, L. Shannon, H. D. Cunningham, S. Smith, F. Li, B. C. Fassold, and C. M. Vines, Arrestin 3 mediates endocytosis of CCR7 following ligation of CCL19 but not CCL21, J. Immunol. **181**, 4723 (2008).

[39] V. Obrien, Eggs and other deformed spheroids in Stokes flow (numerical IBM 7094 computer program calculations for viscous flow fields for nonspherical bodies), APL Technical Digest **4**, 11 (1965).

[40] T. Frankel, *The Geometry of Physics: An Introduction* (Cambridge University Press, Cambridge, England, 2011).

[41] D. D. Patel, W. Koopmann, T. Imai, L. P. Whichard, O. Yoshie, and M. S. Krangel, Chemokines have diverse abilities to form solid phase gradients, Clin. Immunol. **99**, 43 (2001).

[42] A. Sahni, T. Odrljin, and C. W. Francis, Binding of basic fibroblast growth factor to fibrinogen and fibrin, J. Biol. Chem. **273**, 7554 (1998).

[43] A. Sahni, M. Guo, S. K. Sahni, and C. W. Francis, Interleukin-1β but not IL-1α binds to fibrinogen and fibrin and has enhanced activity in the bound form, Blood **104**, 409 (2004).

[44] S. Lee, S. M. Jilani, G. V. Nikolova, D. Carpizo, and M. L. Iruela-Arispe, Processing of VEGF-A by matrix metalloproteinases regulates bioavailability and vascular patterning in tumors, J. Cell Biol. **169**, 681 (2005).

[45] A. C. Shieh, H. A. Rozansky, B. Hinz, and M. A. Swartz, Tumor cell invasion is promoted by interstitial flow-induced matrix priming by stromal fibroblasts, Cancer Res. **71**, 790 (2011).

[46] W. J. Polacheck, J. L. Charest, and R. D. Kamm, Interstitial flow influences direction of tumor cell migration through competing mechanisms, Proc. Natl. Acad. Sci. U.S.A. **108**, 11115 (2011).

[47] J. Desponds, M. Vergassola, and A. M. Walczak, Hunchback promoters can readout morphogenetic positional information in less than a minute, arXiv:1906.08317.